PHYSICAL REVIEW A VOLUME 22, NUMBER 3 SEPTEMBER 1980

Analysis of Beutler-Fano autoionizing resonances in the rare-gas atoms using the relativistic multichannel quantum-defect theory

W. R. Johnson
Physics Department, University of Notre Dame, Notre Dame, Indiana 46556

K. T. Cheng
Argonne National Laboratory, Argonne, Illinois 60439

K.-N. Huang
Physics Department, University of Notre Dame, Notre Dame, Indiana 46556

M. Le Dourneuf
Observatorie de Paris, Section d'Astrophysique, 92190 Meudon, France
(Received 31 March 1980)

The Beutler-Fano autoionizing resonances in the rare-gas atoms argon, krypton, and xenon are studied using the relativistic multichannel quantum-defect theory (MQDT). Dynamical parameters for the MQDT analyses are obtained from an *ab initio* relativistic-random-phase-approximation calculation. The position and profile of these resonances are in good agreement with experimental measurements. Angular distribution and spin polarization of photoelectrons in the resonance regions are also studied and are in close agreement with recent measurements.

I. INTRODUCTION

In this paper we report results of *ab initio* calculations of the Beutler-Fano autoionization resonances in argon, krypton, and xenon and compare our results with recent experimental measurements. The dipole-allowed single-electron excitation spectrum of the noble gases consists of five interacting Rydberg series. Three of these series arise from excitation of an outer $p_{3/2}$ electron to $ns_{1/2}$, $nd_{3/2}$, or $nd_{5/2}$ states; these three series converge to the $^2P^o_{3/2}$ ground state of the ion. The remaining two series arise from excitation of an outer $p_{1/2}$ electron to $ns_{1/2}$ or $nd_{3/2}$ states (termed ns' and nd' states in the sequel) and converge to the lowest excited $^2P^o_{1/2}$ state of the ion. The latter two series have members which lie in the continuum above the $^2P^o_{3/2}$ ionization threshold and are therefore subject to autoionization. The photoionization cross section in the energy interval between $^2P^o_{3/2}$ and $^2P^o_{1/2}$ thresholds exhibits two resonant series; a sharp series associated with excitations to the ns' states and a diffuse series associated with excitations to nd' states.

Autoionization resonances between the $^2P^o_{3/2}$ and $^2P^o_{1/2}$ thresholds in argon, krypton, and xenon were first observed by Beutler[1] and analyzed by Fano.[2] For argon, wavelengths of members of the ns' and nd' series and widths of the nd' resonances have been determined experimentally by Yoshino[3] and by Radler and Berkowitz.[4] Measurements of the absolute photoionization cross section for argon in the resonance region have been carried out by a number of workers[5-8] and are summarized by Hudson and Kiefer.[9]

Experimental measurements of the wavelengths of the ns' and nd' resonances for krypton have been reported by Yoshino and Tanaka,[10] and by Radler and Berkowitz,[4] while absolute cross sections for krypton have been determined by Metzger and Cook[7] and by Huffman, Tanaka, and Larrabee.[11] Locations of a number of ns' and nd' resonances are listed by Radler and Berkowitz[4] and by Moore[12] for xenon, and absolute photonionization cross sections for xenon in the resonance region have been reported by various groups.[5,7,13]

The more recent theoretical treatments of Beutler-Fano resonances have been based on multichannel quantum-defect theory (MQDT).[14] Discrete states and autoionization resonances in xenon were studied by Lu,[15] who employed empirically determined MQDT parameters. These studies were extended to argon by Lee and Lu.[16] The MQDT parameters for argon were also determined from an *ab initio* calculation by Lee,[17] who solved the many-electron Schrödinger equation in a limited spherical region. Further studies of autoionization in xenon and krypton using empirical MQDT parameters have been carried out by Geiger.[18,19]

Measurements of the angular-distribution asymmetry parameter β for xenon have been reported by Samson and Gardner.[20] The experimental values of β have been compared with theoretical MQDT values by Dill[21] and by Geiger.[18,19] The angular-distribution parameters depend on relative phases as well as magnitudes of photonioization amplitudes, so that comparisons of MQDT predictions for angular distributions with experiment

place additional constraints on the MQDT parameters beyond those already included in cross-section comparisons.

Studies of spin polarization of photoelectrons also provide sensitive tests of MQDT parameters. Calculations of the spin polarization for xenon and argon in the MQDT formalism have been given by Lee.[22] These calculations have recently been subjected to experimental tests by Heinzmann *et al.*,[23] who measure the total spin polarization of xenon in the autoionizing region of the spectrum. In the following paragraphs we present theoretical studies of the Beutler-Fano resonances based on *ab initio* calculations of the MQDT parameters using the relativistic random-phase approximation (RRPA). A detailed account of the theory behind the present calculations is given in a previous paper.[24]

The Beutler-Fano resonances in Ne have already been considered using the present technique.[25] Here, we concentrate on the applications of the theory to argon, krypton, and xenon. In Sec. II we summarize the formulas required to calculate the photoabsorption cross section in the autoionization region. Our calculated MQDT parameters are then presented, along with angular distributions and spin polarization in Sec. III.

These studies should provide an aid to the understanding of systematic features of the Beutler-Fano resonances. Further experimental studies of the resonances, especially measurements of angular distributions and spin polarization, should provide sensitive tests of the theoretical MQDT parameters.

II. THEORETICAL CONSIDERATIONS

The theory of photoionization of atoms by polarized photons has been discussed by several authors.[22,26-30] We restrict our attention here to photoionization by circularly polarized incident radiation. To describe photoionization by unpolarized incident radiation, one must average the results presented below over the two states of circular polarization. For low-energy photoionization, where the electric dipole approximation is valid, the photoelectron angular distribution is given by

$$\frac{d\sigma}{d\Omega}=\frac{\sigma}{4\pi}[1-\tfrac{1}{2}\beta P_2(\cos\theta)]\,, \tag{1}$$

where θ is the angle between the photon momentum $\vec{k}$ and the electron momentum $\vec{p}$. In Eq. (1), σ is the photoionization cross section and β is a parameter which measures the asymmetry in the angular distribution. The polarization vector $\vec{P}$ of the photoelectron is conveniently expressed in a coordinate system with z axis along the photoelectron momentum vector $\vec{p}$, with y axis normal to the production plane (in the direction $\vec{k}\times\vec{p}$), and with x axis in the production plane, but perpendicular to $\vec{p}$ [in the direction $(\vec{k}\times\vec{p})\times\vec{p}$]. The components of $\vec{P}$ in this coordinate system are[30]

$$P_x=\pm\frac{\xi\sin\theta}{1-\frac{1}{2}\beta P_2(\cos\theta)}\,, \tag{2}$$

$$P_y=\frac{\eta\sin\theta\cos\theta}{1-\frac{1}{2}\beta P_2(\cos\theta)}\,, \tag{3}$$

$$P_z=\pm\frac{\zeta\cos\theta}{1-\frac{1}{2}\beta P_2(\cos\theta)}\,, \tag{4}$$

where the $\pm$ signs refer to incident photons of positive or negative helicity, respectively. The dynamical parameters σ, β, ξ, η, and ζ, which will be discussed explicitly below, are given in terms of reduced matrix elements of the dipole operator. Although we have restricted our discussion to the case of circularly polarized incident radiation, it is worth mentioning that the five dynamical parameters σ, β, ξ, η, and ζ suffice to describe low-energy photoionization for incident radiation of arbitrary polarization.[30]

For unpolarized incident radiation, only the component P_y is nonvanishing. If the incident radiation is circularly polarized, the spin polarization of the total electron flux (in the direction of incident radiation) is given by

$$P_{\rm tot}=\pm\delta\,, \tag{5}$$

where

$$\delta=\tfrac{1}{3}(\zeta-2\xi)\,. \tag{5a}$$

For the present purposes we consider photoionization of rare gases by photons with energy above the $^2P^o_{3/2}$ threshold, but below the $^2P^o_{1/2}$ threshold. In this energy region there are three open channels corresponding to the excitation of an outer $p_{3/2}$ electron to $s_{1/2}$, $d_{3/2}$, or $d_{5/2}$ continuum states. We label the reduced matrix element of the dipole operator in these channels by the photoelectron angular momentum $j=\frac{1}{2}$, $\frac{3}{2}$, and $\frac{5}{2}$. These dipole amplitudes D_j may be easily obtained from the MQDT. We write[24]

$$D_j=\sum_{\rho=1}^{3}\bar{T}^{\rho}_j e^{i\pi\tau_\rho}\bar{D}_\rho\,, \tag{6}$$

where $\pi\tau_\rho$ are the short-range eigenphases of the three open eigenchannels, $\bar{D}_\rho$ are the corresponding eigenamplitudes, and $\bar{T}^o_j$ is the orthogonal transformation matrix between the eigenchannels ($\rho=1,2,3$) and the open channels ($j=\frac{1}{2},\frac{3}{2},\frac{5}{2}$). The amplitudes D_j are determined from solutions to the RRPA equations, which satisfy outgoing-wave boundary conditions in the open channels. The quantities τ_ρ, $\bar{D}_\rho$, and $\bar{T}^o_j$ all may be obtained from

the multichannel quantum-defect parameters μ_α, D_α, and $U_{i\alpha}(i,\alpha=1,\ldots,5)$, using the procedures described in detail in Ref. 24.

We may express the dynamical parameters σ, β, ξ, η, and ζ in terms of the amplitudes D_j (atomic units are used) by

$$\sigma = 2\pi^2\alpha\frac{df}{dE} = \frac{4\pi^2\alpha}{3}\omega\bar{\sigma}\,, \tag{7}$$

$$\bar{\sigma} = |D_{1/2}|^2 + |D_{3/2}|^2 + |D_{5/2}|^2\,, \tag{8}$$

$$\beta = [-\tfrac{4}{5}|D_{3/2}|^2 + \tfrac{4}{5}|D_{5/2}|^2 - (1/\sqrt{5})(D_{1/2}D^*_{3/2} + \text{c.c.}) - (3/\sqrt{5})(D_{1/2}D^*_{5/2} + \text{c.c.}) + \tfrac{3}{5}(D_{3/2}D^*_{5/2} + \text{c.c.})]\bar{\sigma}^{-1}\,, \tag{9}$$

$$\xi = [\tfrac{1}{2}|D_{1/2}|^2 + \tfrac{2}{5}|D_{3/2}|^2 - \tfrac{9}{10}|D_{5/2}|^2 - \tfrac{1}{4}\sqrt{5}(D_{1/2}D^*_{3/2} + \text{c.c.}) + \tfrac{9}{20}(D_{3/2}D^*_{5/2} + \text{c.c.})\bar{\sigma}^{-1}\,, \tag{10}$$

$$\eta = i[(3/4\sqrt{5})(D_{1/2}D^*_{3/2} - \text{c.c.}) - (3/2\sqrt{5})(D_{1/2}D^*_{5/2} - \text{c.c.}) + \tfrac{3}{4}(D_{3/2}D^*_{5/2} - \text{c.c.})]\bar{\sigma}^{-1}\,, \tag{11}$$

$$\zeta = [-\tfrac{1}{2}|D_{1/2}|^2 + \tfrac{1}{5}|D_{3/2}|^2 + \tfrac{3}{10}|D_{5/2}|^2 - \tfrac{1}{2}\sqrt{5}(D_{1/2}D^*_{3/2} + \text{c.c.}) - \tfrac{9}{10}(D_{3/2}D^*_{5/2} + \text{c.c.})]\bar{\sigma}^{-1}\,. \tag{12}$$

Our calculation of the angular distribution and spin polarization of photoelectrons within the resonance region involves several computational steps. First, we solve the many-electron problem describing photoexcitation using the RRPA to find the smooth MQDT parameters μ_α, D_α, and $U_{i\alpha}$ at a number of energies in the resonance region. For practical reasons we must limit these RRPA calculations to include only a few important interchannel correlations. In the case of argon, we include the correlations within and between the $3s$ and $3p$ shells, and we treat the inner shells in a frozen-core approximation. The justification for this truncation has been discussed before.[31] For krypton, we include the $4s$, $4p$, and $3d$ shells in the dynamical calculation, while for xenon we include $5s$, $5p$, and $4d$ shells. The importance of including inner d-shell correlations in the RPA calculations has been discussed by Amusia[32]; we illustrate the effect of $4d$ correlations on the Beutler-Fano resonances of Xe in the following section.

Once the MQDT parameters have been determined from the RRPA calculations, we carry out the analysis described in Ref. 24 to determine the eigenphases and eigenamplitudes in the open channels, $\bar{D}_\rho$ and τ_ρ, and the transformation matrix $\bar{T}^\rho_j$. The production amplitudes D_j and the five parameters σ, β, ξ, η, and ζ describing photoionization are then easily obtained using Eqs. (7) through (12).

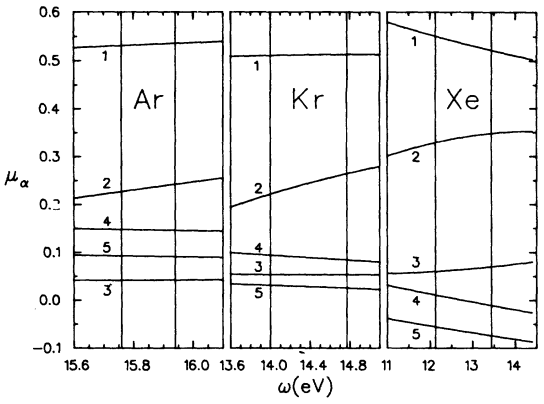

FIG. 1. Eigen-quantum defects μ_α plotted as functions of photon energy ω across the first two thresholds of the rare-gas atoms argon, krypton, and xenon.

In RRPA calculations the theoretical photoionization thresholds are given by the eigenvalues of the Dirac-Fock equations for the atomic ground state. Since these theoretical thresholds are only in fair agreement with experimental thresholds, we adopt in the following section the procedure of aligning the theoretical and experimental profiles at the second thresholds when presenting our comparisons with experimental data.

III. RESULTS AND DISCUSSIONS

As discussed in previous papers,[14-16,24] MQDT allows one to characterize the dynamics of photoionization processes in terms of a few parameters: the eigen-quantum defects μ_α, the eigen-dipole amplitudes D_α, and the transformation matrices $U_{i\alpha}$. These parameters are slowly varying functions of energy near the thresholds, so that they can be interpolated or extrapolated in the autoion-

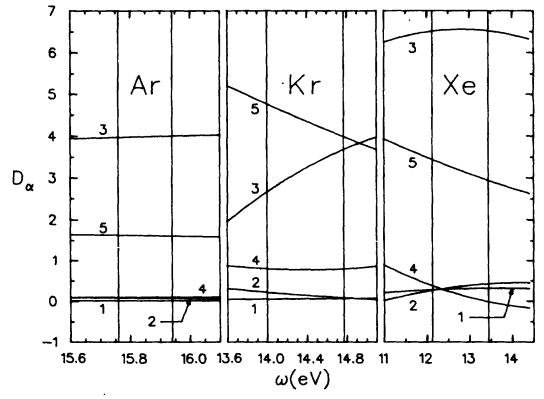

FIG. 2. Eigen-dipole amplitudes D_α plotted as functions of photon energy ω across the first two thresholds of the rare-gas atoms argon, krypton, and xenon.

TABLE I. Transformation matrices $U_{i\alpha}$, eigen-quantum defects μ_α, and eigen-dipole amplitudes D_α (in atomic units) at the $^2P^0_{1/2}$ thresholds of the rare-gas atoms argon, krypton, and xenon.

		Ar					Kr					Xe				
	i/α	1	2	3	4	5	1	2	3	4	5	1	2	3	4	5
$U_{i\alpha}$	1	0.056	0.001	0.041	−0.555	0.829	−0.086	−0.003	0.350	0.500	−0.787	0.074	−0.010	−0.146	0.346	0.924
	2	0.734	0.625	0.255	0.073	−0.014	−0.737	−0.615	−0.223	−0.136	−0.103	0.720	−0.633	0.279	−0.050	−0.002
	3	−0.546	0.333	0.767	−0.045	−0.032	0.546	−0.349	−0.671	−0.007	−0.360	−0.563	−0.323	0.743	0.121	0.113
	4	0.079	−0.003	−0.014	−0.826	−0.558	−0.119	0.006	−0.326	0.846	0.405	0.080	0.003	−0.034	0.929	−0.360
	5	0.392	−0.706	0.587	0.046	−0.024	−0.371	0.707	−0.521	−0.126	−0.274	0.391	0.704	0.590	0.011	0.065
μ_α		0.536	0.242	0.042	0.145	0.090	0.513	0.260	0.053	0.085	0.026	0.521	0.348	0.070	−0.011	−0.074
D_α		0.006	0.067	4.005	0.095	1.605	0.061	0.092	3.572	0.778	4.084	0.314	0.424	6.517	−0.021	2.938

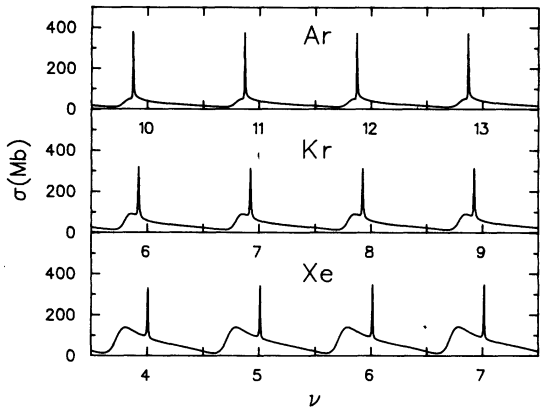

FIG. 3. Photoionization cross sections σ plotted against the effective quantum number ν.

ization region. To show the energy dependence of the MQDT parameters between the $^2P^o_{3/2}$ and $^2P^o_{1/2}$ thresholds of the rare gases argon, krypton, and xenon, we plot in Figs. 1 and 2 the values of μ_α and D_α obtained from the RRPA as functions of photon energies. As one can see from these figures, μ_α and D_α vary smoothly across the first two thresholds and are nearly linear functions of photon energies.

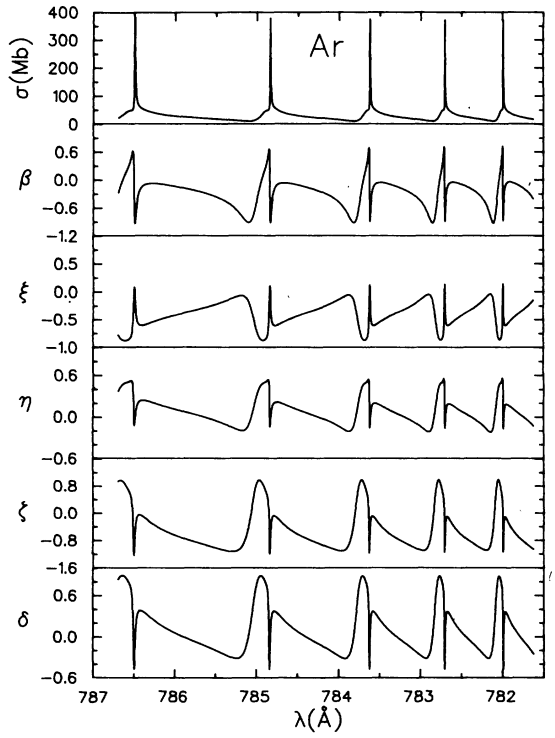

FIG. 4. Photoionization cross sections σ, angular-distribution asymmetry parameters β, and spin-polarization parameters ξ, η, ζ, and δ plotted as functions of photon wavelength λ in the autoionization region of argon.

For low-energy photoionization, the LS coupling scheme provides a good approximate description of the eigenchannels. In Fig. 2 the two strong channels ($\alpha = 3, 5$) with sizeable dipole amplitudes D_α correspond roughly to the dipole-allowed excitations from the ^1S ground state to the $(p^5d)^1P^o$ and $(p^5s)^1P^o$ states, respectively, while the three remaining weak channels ($\alpha = 1, 2, 4$) are associated with the forbidden excitations to the $(p^5d)^3P^o$, $(p^5d)^3D^o$, and $(p^5s)^3P^o$ states, respectively. A general trend here is the steady increase in the size of the corresponding eigenamplitudes D_α from argon to krypton to xenon, resulting in the increase in cross sections among these atoms, as shown below. The rapid increase in the magnitude of the three weak channels reflects the increasing importance of spin-orbit interactions in heavy atoms. The assignment of the jj-coupled channel indices i and the eigenchannel indices α are given by

$i, \alpha =$	1	2	3	4	5
i	$(^2P^o_{3/2})s_{1/2}$	$(^2P^o_{3/2})d_{3/2}$	$(^2P^o_{3/2})d_{5/2}$	$(^2P^o_{1/2})s_{1/2}$	$(^2P^o_{1/2})d_{3/2}$
α	$(p^5d)^3P^o$	$(p^5d)^3D^o$	$(p^5d)^1P^o$	$(p^5s)^3P^o$	$(p^5s)^1P^o$

Numerical values of μ_α, D_α, and $U_{i\alpha}$ at the $^2P^o_{1/2}$ thresholds of argon, krypton, and xenon are given in Table I.

In Fig. 3, the cross sections in the autoionizing regions of argon, krypton, and xenon are plotted as functions of the effective quantum number ν defined in the preceding paper.[24] (Nonrelativistically, ν is defined in terms of the energy ϵ relative to the $^2P^o_{1/2}$ threshold as $\epsilon = -\frac{1}{2}\nu^{-2}$.) One sees in these plots that the Beutler-Fano profiles are practically the same along the Rydberg series. This is not surprising in view of the weak energy dependence of the quantum-defect parameters. The implication of these regularities is that physical observables such as cross sections, asymmetry param-

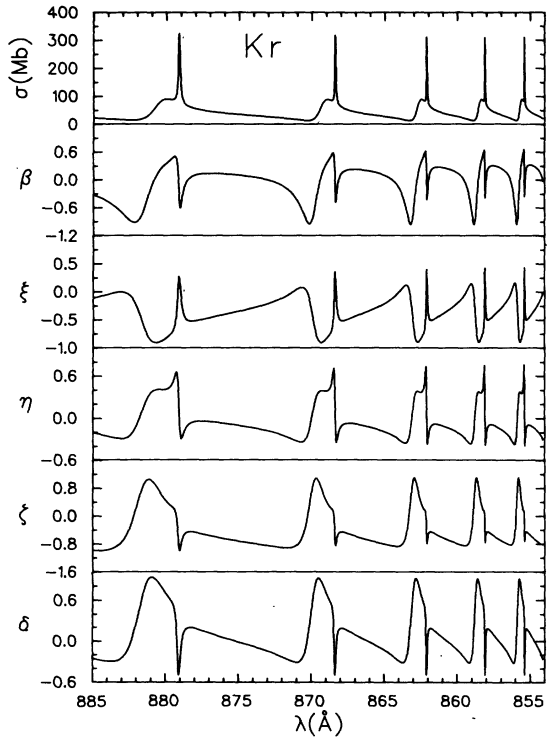

FIG. 5. Photoionization cross sections σ, angular-distribution asymmetry parameters β, and spin-polarization parameters ξ, η, ζ, and δ plotted as functions of photon wavelength λ in the autoionization region of krypton.

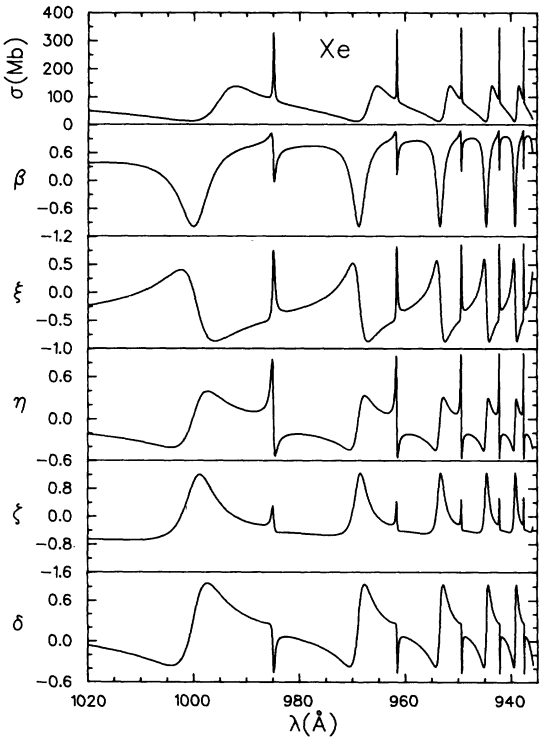

FIG. 6. Photoionization cross sections σ, angular-distribution asymmetry parameter β, and spin-polarization parameters ξ, η, ζ, and δ plotted as functions of photon wavelength λ in the autoionization region of xenon.

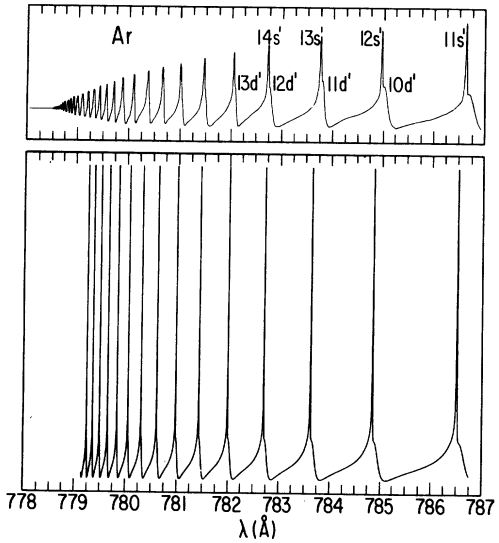

FIG. 7. Photoionization spectra of argon between the $^2P^o_{3/2}$ and $^2P^o_{1/2}$ thresholds. The upper graph shows experimental data by Radler and Berkowitz[4] with a photon resolution width of 0.02 Å, and the lower graph shows results of this calculation.

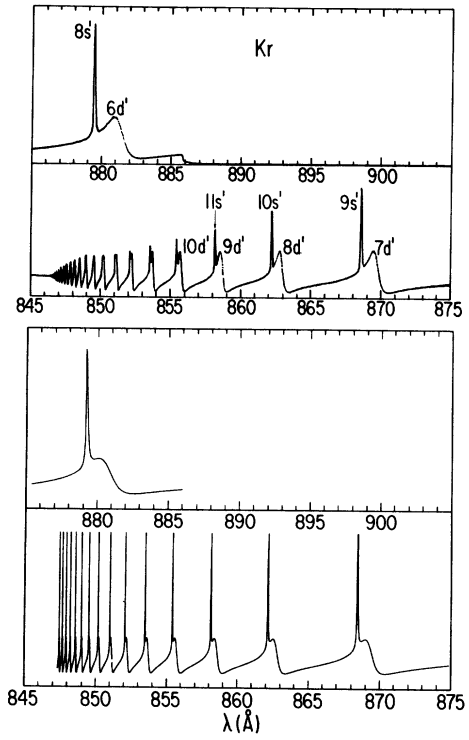

FIG. 8. Photoionization spectra of krypton between the $^2P^o_{3/2}$ and $^2P^o_{1/2}$ thresholds. The upper graph shows experimental data obtained by Berkowitz (Ref. 33) with a photon resolution width of 0.07 Å, and the lower graph shows results of this calculation.

eters, and spin polarizations in the autoionizing region are characterized by their respective profiles at the first few resonances.

For argon, the sharp ns' resonances almost coincide with the broad nd' ones. The two resonances depart from each other in krypton, and they are well separated in xenon. From argon to krypton to xenon, one also sees that the magnitudes of the broad nd' resonances are increasing, while those of the ns' series remain fairly constant.

In Fig. 4 results of our present calculations on cross sections σ, angular asymmetry parameters β, and spin-polarization parameters ξ, η, ζ, and δ for argon are plotted as functions of photon wavelength λ. Similar plots for krypton and xenon are shown in Figs. 5 and 6, respectively. Because of the repetition of these parameters along the Rydberg series, only those results for the first few resonances are presented. These parameters, σ, β, ξ, η, ζ, and δ show two distinct patterns: sharp changes at the locations of ns' resonances, superimposed on slower changes arising from the nd' series.

In Figs. 7, 8, and 9, we compare our calculated resonance profiles with recent experimental measurements by Radler and Berkowitz[4] for argon,

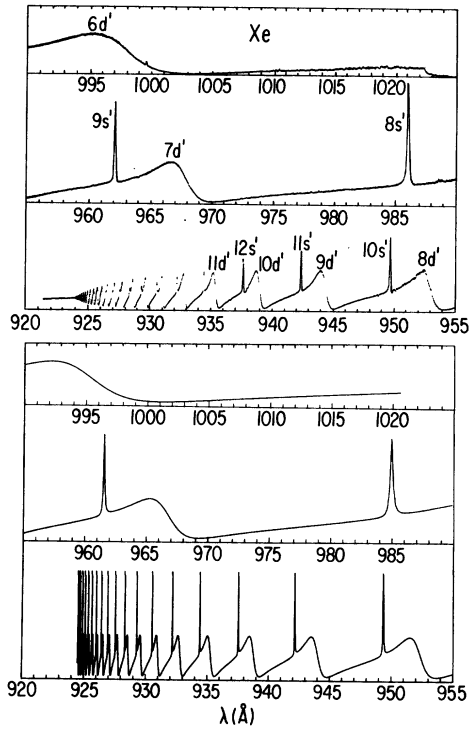

FIG. 9. Photoionization spectra of xenon between the $^2P^o_{3/2}$ and $^2P^o_{1/2}$ thresholds. The upper graph shows experimental data obtained by Eland (Ref. 33) with a photon resolution width of 0.07 Å, and the lower graph shows results of this calculation.

and by Berkowitz[33] for krypton and xenon. As can be seen from these figures, the general features of the autoionization profiles are well represented by the present calculations; however, there are minor discrepancies which should be noted. First, the positions of the resonances are slightly shifted. This shift is most pronounced near the $^2P^o_{3/2}$ threshold, and the theoretical resonances are located at shorter wavelengths than the experimental ones. Second, there is a rapid decrease in the size of the ns' peaks in the experimental spectrum which does not occur in the theoretical spectrum. For higher members of the Rydberg series, it is clear that the overall decrease in experimental resonance amplitudes is due to finite instrumental resolution; however, it is not clear whether the apparent decrease in the relative size of the experimental peaks for the first few resonances is a real effect or is due to instrumentation. From the theoretical point of view, it is difficult to understand a real decrease of the size along the Rydberg series, since such a decrease would imply a rapid change in the associated quantum-defect parameters in a relatively small energy region.

A third problem which can be noted is that the relative separation of the ns' and nd' resonances is somewhat different in the theoretical and experimental spectra. We believe that this problem is due, at least in part, to the limited correlation included in the present RRPA calculation. To illustrate the influence of inter-shell correlations on the resonance profiles, we present in Fig. 10 a comparison of two theoretical results in the $(9d', 11s')$ region of the xenon spectrum. The first of these theoretical curves is a portion of the spectrum presented before in Fig. 9, which includes correlations from the $5p$, $5s$, and $4d$ shells. In the second curve, the $4d$ and $5s$ correlations are omitted. We find only an insignificant shift in the location of the theoretical resonance positions (less than 0.1 Å in this region), and for comparison purposes we simply line up the $11s'$ peaks in Fig. 10. As is apparent from the figure, the inclusion of $4d$ correlation increases the magnitude of the $9d'$ resonance and sharpens its profile. To compare with experiment, we superimpose on Fig. 10 the observed spectrum[33] in this region by first lining up the $11s'$ peak and then by scaling the experimental data to agree with theory on the shorter wavelength side of the $9d'$ resonance. The point here is that inter-shell correlation from $4d$ (and to a lesser extent, $5s$) brings the theoretical profile of the $9d'$ resonances into closer agreement with observation. Also, because of the sharpening of the theoretical $9d'$ profile, there is an apparent increase in the separation of $9d'$ and $11s'$ resonances. This increased separation on including inter-shell correlations is in the right direction, but is still insufficient to account entirely for the observed separation.

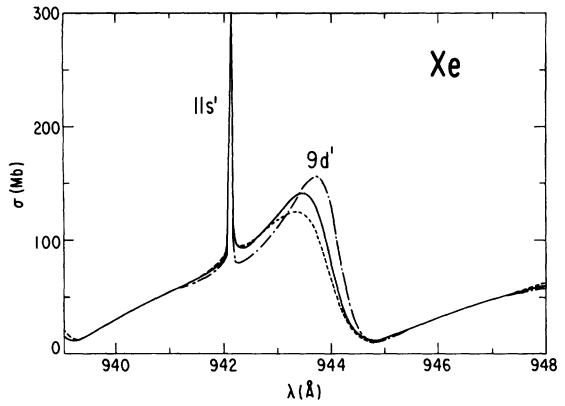

FIG. 10. Photoionization cross sections σ plotted against photon wavelength λ in the autoionization region of xenon. The solid curve is the result of this calculation, including correlations between the $5p$, $5s$, and $4d$ shells. The dashed curve is the result of this calculation with the $5p$-shell correlations only. The dash-dot curve is the experimental data shown in Fig. 9 scaled to match theoretical curves on the shorter-wavelength side of the $9d'$ resonance. All curves are lined up at the $11s'$ resonance for comparison purposes.

In Fig. 11 we compare our theoretical predictions of the angular-distribution β parameters for xenon near the $(6d', 8s')$ resonances with the measurements of Samson and Gardner.[20] To compare the profile of the β parameter, we align the theoretical and experimental $8s'$ resonances. The general agreement with experiment is good, although the data are not sufficiently detailed to reveal the structure of β near the $8s'$ resonance. We also

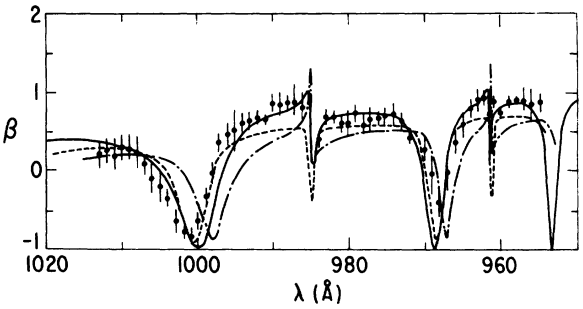

FIG. 11. Angular-distribution asymmetry parameters β plotted against photon wavelength λ in the autoionization region of xenon. Dots are experimental data by Samson and Gardner (Ref. 20). The solid curve is the result of this calculation. The dash-dot and the dashed curves are MQDT calculations by Dill (Ref. 21) and Geiger (Ref. 19), respectively. All curves are lined up at the $8s'$ resonances for comparison purposes.

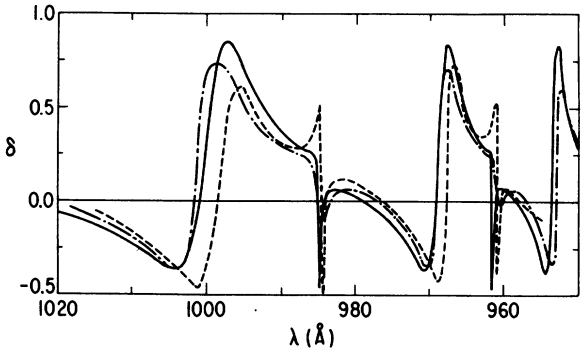

FIG. 12. Total spin-polarization parameters δ plotted against photon wavelengths λ in the autoionization region of xenon. The dash-dot curve is the experimental data by Heinzmann *et al.* (Ref. 23). The solid curve is the result of the present calculation. The dashed curve is the MQDT calculation of Lee (Ref. 22). All curves are lined up at the $8s'$ resonances for comparison purposes.

show in the same graph two MQDT calculations by Dill[21] and by Geiger,[19] based on empirical quantum-defect parameters. Once again, the overall agreement is good, except for the detailed features near the $8s'$ resonances.

In Fig. 12 our results on the total spin-polarization parameter δ in xenon near the $(6d', 8s')$ resonances are compared with recent experimental measurements of Heinzmann *et al.*[23] In the same figure, we give the results of a MQDT calculation by C. M. Lee.[22] Again, as in the case of the β parameter, the general agreement between theoretical and experimental profiles is good. The two theoretical profiles differ somewhat at the $8s'$ resonance. In this case, the experimental profile at the $8s'$ resonance has been given in detail and is in somewhat better agreement with the present calculation.

In the above paragraphs, we have presented our MQDT studies of the Beutler-Fano profiles for the rare gases argon, krypton, and xenon using dynamical parameters determined from the RPPA. We have found that the systematic features of the profiles are in good agreement with existing experimental data. These comparisons show the utility of the MQDT–RRPA approach in predicting complex spectra involving strongly interacting channels. For further comparisons, it would be desirable to have measurements of β and δ parameters for krypton and argon. Measurements of the η parameter, such as those made at higher photon energies by Heinzmann *et al.*,[34] would also be useful since they would compliment the existing experimental data in the resonance region.

ACKNOWLEDGMENTS

The authors would like to thank Dr. J. Berkowitz for communicating unpublished data and for helpful discussions. We are also grateful to Dr. K. Yoshino and Dr. U. Heinzmann for helpful correspondence. The work of W. R. J. and K.-N. Huang are supported in part by the National Science Foundation under Grant No. PHY79-09229. The work of K. T. C. is supported by the U. S. Department of Energy. One of us (W.R.J.) thanks the Argonne National Laboratory for an appointment.

[1]H. Beutler, Z. Phys. 93, 177 (1935).
[2]U. Fano, Nuovo Cimento 12, 154 (1935).
[3]Kouichi Yoshino, J. Opt. Soc. Am. 60, 1220 (1970).
[4]K. Radler and J. Berkowitz, J. Chem. Phys. 70, 216 (1979); 70, 221 (1979).
[5]R. E. Huffman, Y. Tanaka, and J. C. Larrabee, J. Chem. Phys. 39, 902 (1963).
[6]R. D. Hudson and V. L. Carter, J. Opt. Soc. Am. 58, 227 (1968).
[7]P. H. Metzger and G. R. Cook, J. Opt. Soc. Am. 55, 516 (1965).
[8]Po Lee and G. L. Weisler, Phys. Rev. 99, 540 (1955).
[9]R. D. Hudson and L. J. Kiefer, At. Data 2, 205 (1971).
[10]K. Yoshino and Y. Tanaka, J. Opt. Soc. Am. 69, 159 (1979).
[11]R. E. Huffman, Y. Tanaka, and J. C. Larrabee, Appl. Opt. 15, 947 (1963).
[12]C. E. Moore, *Atomic Energy Levels NSRDS-NBS* (U.S. Government Printing Office, Washington, D.C., 1971), Vol. III, pp. 113–117.
[13]F. M. Matsunaga, K. Watanabe, and R. S. Jackson, J. Quant. Spectrosc. Radiat. Transfer 5, 329 (1965).
[14]M. J. Seaton, Proc. Phys. Soc. London 88, 801 (1966); U. Fano, Phys. Rev. A 2, 353 (1970).
[15]K. T. Lu, Phys. Rev. A 4, 579 (1971).
[16]Chia-Ming Lee and K. T. Lu, Phys. Rev. A 8, 1241 (1973).
[17]C. M. Lee, Phys. Rev. A 10, 584 (1974).
[18]J. Geiger, Z. Phys. A 276, 219 (1976).
[19]J. Geiger, Z. Phys. A 282, 129 (1977).
[20]J. A. R. Samson and J. L. Gardner, Phys. Rev. Lett. 31, 1327 (1973).
[21]D. Dill, Phys. Rev. A 7, 1976 (1973).
[22]C. M. Lee, Phys. Rev. A 10, 1598 (1974).
[23]U. Heinzmann, F. Schäfers, K. Thimm, A. Wolcke, and J. Kessler, J. Phys. B 12, L679 (1979).
[24]C. M. Lee and W. R. Johnson, Phys. Rev. A 22, 979 (1980).
[25]W. R. Johnson and M. Le Dourneuf, J. Phys. B 13, L13 (1980).
[26]B. Brehm, Z. Phys. 242, 195 (1971).
[27]V. L. Jacobs, J. Phys. B 5, 2257 (1972).
[28]N. A. Cherepkov, Zh. Eksp. Teor. Fiz. 38, 933 (1974) [Sov. Phys.—JETP 38, 463 (1974)]; J. Phys. B 12,

1279 (1979).
[29]R. H. Pratt, A. Ron, and H. K. Tseng, Rev. Mod. Phys. 45, 273 (1973).
[30]K.-N. Huang, Phys. Lett. 77A, 133 (1980); Phys. Rev. A 22, 223 (1980).
[31]W. R. Johnson and K. T. Cheng, Phys. Rev. A 20, 978 (1979).
[32]M. Ya. Amusia and N. A. Cherepkov, Case Stud. At. Phys. 5, 47 (1975).
[33]See J. Berkowitz, *Photoabsorption, Photoionization, and Photoelectron Spectroscopy* (Academic, New York, 1979), pp. 177 and 181.
[34]U. Heinzmann, G. Schönhense, and J. Kessler, Phys. Rev. Lett. 42, 1603 (1979).